Displacement Spikes in Cubic Metals. I. α-Iron, Copper, and Tungsten

J. R. BEELER, JR.
Nuclear Materials and Propulsion Operation, General Electric Company, Cincinnati, Ohio
(Received 19 May 1966)

The production of an isolated displacement spike by a collision cascade in α-iron, tungsten, and copper at 0°K and the annealing of displacement spikes in α-iron at temperatures up to 250°C were studied using the computer-experiment (simulation) method. Collision-cascade simulation in the associated body-centered-cubic (bcc) and face-centered-cubic (fcc) arrays of atoms was based on the approximation of assuming a branching sequence of binary-collisions. The primary knock-on atom (PKA) displacement efficiency was found to be a decreasing function of PKA energy, in contrast to the constant displacement efficiency given by structureless solid models. This effect was caused predominantly by damage-production interference among different parts of the cascade. Long-range channeling (range $\geq$ 1000 Å) played a very minor role in the decrease of the PKA displacement efficiency with increasing PKA energy, in bcc metals and none at all in copper. Quasichanneling events were common and greatly influenced the development of a displacement spike along ⟨110⟩ directions in bcc metals. In this regard, the dimensions of a cascade were determined by the ranges of quasichanneled higher order knock-on atoms in the cascade rather than by the PKA range. The preferred directions for long-range self-channeling were also ⟨110⟩. The calculations suggest that in α-iron and tungsten, only those displacement spikes that would contain clusters of $\geq$10 vacancies at an irradiation temperature of 0°K survive thermal annealing at room-temperature irradiation. Specifically, this means that only those spikes produced by PKA with energies above 3 keV in α iron and above 6 keV in tungsten would contribute surviving defects. The density of displacements in a spike produced at 0°K in α iron was saturated at all PKA energies considered (0.5–20 keV). The temperature dependence of the shape and size of the interstitial-vacancy recombination region in α-iron was determined in part.

1. INTRODUCTION

IT is currently thought that neutron-irradiation effects in a metallic specimen are determined principally by interactions among three imperfection distributions, namely, the impurity-atom distribution, the dislocation distribution, and the distribution of point defects produced directly by irradiation. This being the case, a radiation-damage calculation which gives the spatial distribution of irradiation-produced point defects at the level of atomic dimensions, in addition to the total number of point defects produced, is of immediate interest to the theory of irradiation-damage production and effects. The most simple damage-distribution calculation, pertinent to neutron irradiation, is that for an elastic-collision cascade initiated by a single primary knock-on atom (PKA) in an initially perfect crystal at 0°K. Brinkman[1] has pointed out that the collection of point defects produced by an elastic collision cascade in medium- and heavy-mass metals should be a rather compact assemblage, and introduced the name "displacement spike" for such an assemblage. An attempt to compute the spatial distribution of point defects, at the level of atomic dimensions, in a displacement spike in a pure metal is described in this paper.[2] This was done by generating a branching sequence of binary-atomic-collision events in a cubic array of atoms to simulate the evolution of an atomic-collision cascade in a real crystal with cubic structure. These simulations were performed on a high-speed computer. A damage state produced at 0°K which consists solely of isolated displacement spikes will be called a primary damage state. As will be shown, a primary damage state possesses certain important features which are independent of the energies of the associated cascade-initiating PKA. Computer simulation of damage states which contain overlapping displacement spikes is discussed elsewhere.[3]

Corciovei *et al.*[4] and v. Jan[5] have treated the gross distribution of defects in a displacement spike using a statistical approach based on the work of Holmes and Leibfried.[6] For the most part, the statistical method gives a description of average characteristics and, in practice, has been associated with relatively simple collision models. In contrast, the simulation method allows a detailed study of particular effects and the use of more complicated collision models. One would hope that the two approaches would complement each other. As it turns out, such is the case and in the regions of common applicability the results of the two methods reinforce one another. A detailed description of how the results of the present work and those of the statistical model relate to each other will be given in another paper on the damage state in copper.

The nature of displacement spikes produced in α-iron, tungsten, and copper, at 0°K, and the annealing of dis-

[1] J. A. Brinkman, Am. J. Phys. **24**, 246 (1956).
[2] Preliminary accounts of this work were given at the Symposium on Atomic Collision Cascades, Harwell, 1964 (unpublished) and in Bull. Am. Phys. Soc. **10**, 711 (1965).
[3] J. R. Beeler, Jr., in *Lattice Defects and Their Interactions*, edited by R. R. Hasiguti (Gordon and Breach, Science Publishers Inc., New York, to be published).
[4] A. Corciovei, G. Ghika and D. Grecu, Phys. Rev. **7**, 227 (1962); **8**, 445 (1963); A. Corciovei and A. Babcenco, Phys. Status Solidi **4**, K 1 (1964).
[5] R. v. Jan, Phys. Status Solidi **6**, 925 (1964); **7**, 299 (1964); **8**, 331 (1965).
[6] D. K. Holmes and G. Leibfried, J. Appl. Phys. **31**, 1046 (1960).

placement spikes in α-iron at temperatures below 250°C were studied. PKA energies in the range 0.5–20 keV were considered. The lower limit of this energy range was chosen to furnish overlap with the 0.1–2.5 keV range adopted by Erginsoy *et al.*[7,8] in their many-body calculations. The fact that the elastic-collision assumption is not good above 20 keV, in the case of iron, set the upper limit. An isolated displacement spike was the smallest independent defect aggregate produced by a simulated elastic-collision cascade. This is an essential feature in Brinkman's concept of the displacement spike and the discussion is centered, therefore, primarily on the characteristics of a displacement spike as an entity. The characteristics of the lesser "individual" defect aggregates it contains are treated as secondary considerations. The principal points of interest pertaining to the formation of a displacement spike are the influence of crystal structure on the spatial distribution of defects in a displacement spike and the influence of crystal structure in reducing the damage content of a displacement spike, relative to the damage content predicted by a structureless solid model. The results of simulated thermal annealing, at temperatures between −153° and 250°C, of displacement spikes produced in α-iron at 0°K are summarized. These annealed spikes should closely approximate those produced by irradiation at a temperature in the range −153° to 250°C.

The major part of the article is devoted to α-iron, with selected results for tungsten and copper being presented for purposes of comparison. The damage production results for α iron can be applied to tungsten. Specifically, the average number of displacements produced in tungsten by a PKA with energy E was about that produced in α iron by a PKA with energy $E/2$. There were also certain similarities in the vacancy-cluster size distributions for these two metals. Major differences existed, however, between the characteristics of displacement spikes in copper and those in the two body-centered-cubic (bcc) metals.

2. COMPUTATIONAL MODEL AND PROCEDURE

It was assumed that an atomic-collision cascade could be described as a branching sequence of binary-collision events. A collision cascade of this type is described by Fig. 1. In each event, the collision partners were an energetic knock-on atom and a stationary "target" atom, the latter being either a normally positioned atom or an interstitial. The exit directions for the collision partners and the energy transferred to the target atom (E_t) were computed exactly for the Erginsoy-Vineyard potential,[7] in the case of α iron, and for potential 2 of Gibson *et al.*,[9] in the case of copper.

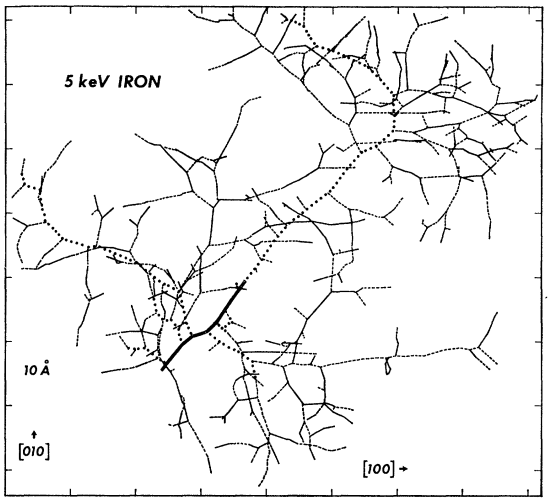

FIG. 1. Projection of the knock-on–atom trajectories in a collision cascade in α iron onto a (001) plane. This cascade was initiated by a 5-keV primary knock-on atom (PKA) ejected from a lattice site at the lower end of the heavy, solid trajectory line. As in this figure, the shape and extent of a cascade was usually determined by quasichanneled trajectories of higher order knock-ons along ⟨110⟩ directions rather than by the form and range of the PKA trajectory.

This was done using the numerical-integration procedure adopted by Robinson and Oen.[10] These potentials were derived by their respective authors from experimental elastic constant and threshold displacement energy data. The potential used in the tungsten calculations was constructed by combining the Thomas-Fermi potential with a potential devised by Johnson.[11] This tungsten potential is defined in the Appendix. The potentials used for tungsten, α-iron, and copper are plotted together in Fig. 2.

To the best of our knowledge, the binary-collision approximation was first used in a computer simulation of collision cascades by Yoshida.[12] He treated cascades in structureless germanium. Robinson and Oen[10] used this approximation in their machine calculations on energetic atom ranges, and Beeler and Besco have used it in machine calculations which describe the effects of crystal structure on the production and distribution of damage in beryllium oxide[13] and α-iron,[14] on the basis of a modified Bohr potential. Both Robinson and Oen, and Beeler and Besco, considered the exact crystal

[7] C. Erginsoy, G. H. Vineyard, and A. Englert, Phys. Rev. **133**, A595 (1964).
[8] C. Erginsoy, G. H. Vineyard, and A. Shimizu, Phys. Rev. **139**, A118 (1965).
[9] J. B. Gibson, A. N. Goland, M. Milgram, and G. H. Vineyard, Phys. Rev. **120**, 1229 (1960).
[10] M. T. Robinson and O. S. Oen, Phys. Rev. **132**, 2385 (1963).
[11] R. A. Johnson, in *Diffusion in Body-Centered Cubic Metals* (American Society for Metals, Cleveland, Ohio, 1965), pp. 357–371.
[12] M. Yoshida, J. Phys. Soc. Japan **16**, 44 (1961).
[13] J. R. Beeler, Jr., and D. G. Besco, in *Radiation Damage in Solids* (International Atomic Energy Agency, Vienna, 1962), Vol. 1, p. 43; J. Phys. Soc. Japan **18**, Suppl. III, 159 (1963); J. Appl. Phys. **34**, 2873 (1963); J. R. Beeler, Jr., J. Nucl. Mat. **15**, 1 (1965).
[14] J. R. Beeler, Jr., and D. G. Besco, Phys. Rev. **134**, A530 (1964); J. Appl. Phys. **35**, 2226 (1964); American Society for Testing and Materials Special Technical Publication No. 380, 1965, pp. 86–104 (unpublished).

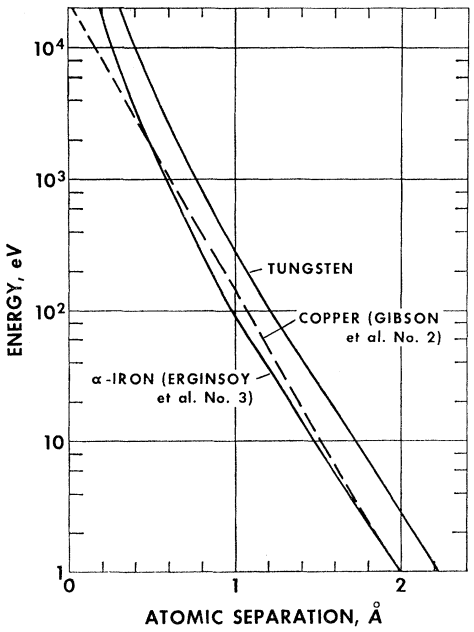

FIG. 2. Interatomic potentials used in collision-cascade simulations for α-iron, copper, and tungsten.

structure in their calculations. Harrison *et al.*[15] have recently compared the binary collision model and an n-body collision model for single collisions between copper atoms in copper, and Erginsoy *et al.*[18] have compared the two models in the case of α-iron. In this regard, Erginsoy *et al.* treated plural- and multiple-collision sequences and their many-body approximation method was more complete than that of Harrison *et al.* Additional aspects of this comparison are given in the paper at hand.

In the present study, elastic collision cascades were simulated for initiating PKA energies of 0.5, 1, 2.5, 5, 10, 15, and 20 keV. Ninety-six independent cascades were simulated for each energy. Each of these cascades was initiated by shooting a PKA from a normal lattice site along a randomly chosen direction into an initially perfect crystal. The initial directions for the initiating PKA were systematically sampled from a uniform distribution in solid angle over the $4\pi/16$-sr symmetry section depicted in Fig. 3, exactly 12 directions being sampled from each of the eight subregions A, $B,\cdots, H$ indicated. The same set of 96 directions was used at each energy. An average resolution of one direction ray per 0.0082 sr is given by this set.

A detailed description of the displacement criteria used in these calculations has been given elsewhere.[16] In short, a target atom receiving more than twice the sublimation energy (E_s) during a collision was ejected from its normal lattice position and sent out into the crystal on a collision trajectory. The initial kinetic energy assigned to an ejected atom was (E_t-2E_s), and its initial direction was that given by the exact collision exit angle calculation. (Recall that E_t is the energy tranferred to the target atom during a collision.) Each ejected atom was allowed to make one collision, regardless of the magnitude of its initial kinetic energy, but otherwise was brought to rest as an interstitial atom when its kinetic energy fell below $2E_s$. If it then satisfied the appropriate Frenkel pair stability conditions (those of Erginsoy *et al.*,[7] for α-iron and tungsten, and those of Gibson *et al.*,[9] for copper) it was considered to be an irreversibly displaced atom in the *current* damage state. Otherwise, it was recombined with the appropriate vacancy.

Interstitial-vacancy recombination in α-iron and tungsten was handled in the following manner: Except for replacement collisions, an atom first found itself in an octahedral interstitial position upon coming to rest. A lattice site for the centroid of a split interstitial configuration was then selected at random from the immediate neighbors of the octahedral position. The stability of the split interstitial thus obtained was tested with respect to recombination with *all* existing vacancies, not just with respect to the vacant site from which the atom had been ejected. These conditions constitute a direction and damage-state-dependent displacement model. A drawing of the 30-site instability region for Frenkel pairs in α-iron, as determined by Erginsoy *et al.*,[7] appears in Fig. 4. These authors found that an interstitial placed at any one of the 24 ⟨111⟩ positions (open circles) or the 6 ⟨100⟩ positions (hatched circles) shown in Fig. 4 would recombine with a vacancy at the center of the instability region (recombination region) at 0°K. A similar treatment of recombination was used in the copper calculations. Except for replacement collisions an energetic atom was first brought to rest at the center of the unit cube and a neighboring split-interstitial position then selected. The 42-site recombination region of Gibson *et al.*[9] was used to test the stability of the interstitial relative to each vacancy. One would expect the size of the recombination region to increase with temperature. This aspect of displacement spike production is discussed briefly in Sec. 5.

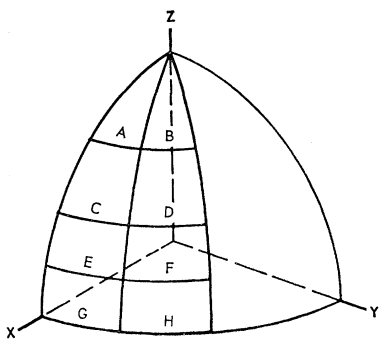

FIG. 3. Initial directions for the PKA were systematically sampled from the eight equal solid-angle increments associated with the areas A–H on the unit sphere shown above.

[15] W. L. Gay and D. E. Harrison, Jr., Phys. Rev. **135**, A1780 (1964); D. E. Harrison, Jr., R. W. Leeds, and W. L. Gay, J. Appl. Phys. **36**, 3154 (1965).

[16] J. R. Beeler, Jr., and D. G. Besco, J. Appl. Phys. **34**, 2873 (1963).

As in our previous damage calculations, the current damage state was always reviewed prior to selecting each target atom and the chronological sequence of the cascade evolution was approximated by scheduling collision events on the basis of knock-on atom velocities.

3. COLLISION-CASCADE STRUCTURE

A. Knock-On–Atom Trajectories

Figure 1 describes a branching sequence of knock-on atom trajectories initiated by a 5-keV primary knock-on atom (PKA) in α iron. The lines in this figure are the projections of the knock-on atom trajectories in a three-dimensional cascade onto a (001) plane. The short heavy bar, with the kink in the middle, represents the trajectory of the initiating PKA and the heavy dotted lines emanating from this bar represent secondary knock-on atom trajectories. The alternately dashed and solid lines, thereafter, denote the trajectories of successively higher order knock-on atoms. The preferred $\langle 110 \rangle$ orientation exhibited by the longer trajectory lines in Fig. 1, appears to be a general characteristic of collision cascades in α-iron and tungsten. This orientation occurred also in earlier calculations for α-iron wherein a Bohr-potential collision diameter and hard-sphere scattering were assumed.[14] The fluctuation about the average range for an energetic atom in copper was much less than that for an equally energetic atom in α-iron and the occurrence of a preferred orientation for long trajectories in copper was observed with a correspondingly smaller frequency.

Channeling[17] events exerted a significant influence on the structure of a collision cascade in α-iron when the energy of the initiating PKA was greater than or equal to 2.5 keV. A detailed description of channeling events, pertinent to this influence, appears in Sec. 5. As illustrated in Fig. 1, the extent of a cascade was usually determined by the ranges of quasichanneled knocked-on atoms of second or higher order rather than by the range of the initiating PKA. This occurred because the number N of knock-on atoms produced in a cascade which are sufficiently energetic to experience channeling is of the order of 10, while there is only one PKA per cascade, and the fact that the average channeling probability $\bar{p}$ for atoms with this energy is relatively large (~ 0.1). This being the case, the average number of channeled knock-ons $N_{\bar{p}}$ per cascade is at least unity and hence at least 10 times greater than the probability (average number) for PKA channeling per cascade.

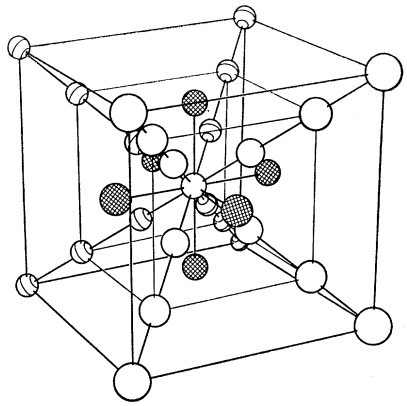

FIG. 4. Atom sites contained in the Erginsoy-Vineyard recombination region for α-iron at 0°K.

In most instances, the PKA energy was completely transferred to secondary knock-on atoms within a distance of 10–80 Å in α-iron and copper for PKA energies in the range $0.5 \leq E \leq 25$ keV. Long-range PKA channeling (range ≥ 1000 Å) occurred with a probability of about 0.05 for PKA energies $E \geq 5$ keV. In these instances, the cascade produced consisted of two or more disjoint subsidiary cascades.

B. Collided-Atom Distribution

A fundamental entity in the study of a displacement spike is the distribution of collided atoms[18] for the associated collision cascade. As will be shown, the manner in which the distribution of defects within a displacement spike evolves depends upon the collided-atom distribution. Because it is the part of a crystal directly affected by a collision cascade, the volume of collided atoms is the appropriate volume for use in computing the average defect density in the associated displacement spike.

The distributions of collided atoms at the centers of two 5-keV collision cascades are shown in Figs. 5 and 6, and that at the center of a 20-keV cascade appears in Fig. 7. Each figure concerns all of the collided atoms in four successive (002) planes, i.e., in a slab region normal to the [001] direction which is two lattice constants ($2a$) thick. In each case, the centroid of the associated collided-atom volume is contained in the region depicted. Each filled circle represents the (x,y) position of a target atom which received at least one collisional energy transfer greater than $2E_s$ (8 eV in α iron). Each open circle represents the position of a target atom which received at least one collisional energy transfer

[17] We will distinguish between two types of channeling in this paper: long-range channeling and quasichanneling. The term long-range channeling pertains to those atom trajectories which extend 1000 Å or more within one of the open, tunnel-like cores present in all crystal structures. These cores are called low-index channels. In fcc crystals they have the directions $\langle 100 \rangle$ and $\langle 110 \rangle$; in bcc crystals they have the directions $\langle 100 \rangle$, $\langle 110 \rangle$, and $\langle 111 \rangle$. Quasichanneling refers to trajectories of lesser extent. For the most part, such trajectories exhibit intermittent low-index channeling and are confined between two closely adjacent atom planes. Atomic displacements are produced during a quasichanneling event but are rarely produced during a long-range channeling event.

[18] In a branching sequence of binary collisions approximation to a collision cascade, the term "collided atom" denotes an atom which received a nonzero energy transfer from either the initiating PKA or an ejected atom.

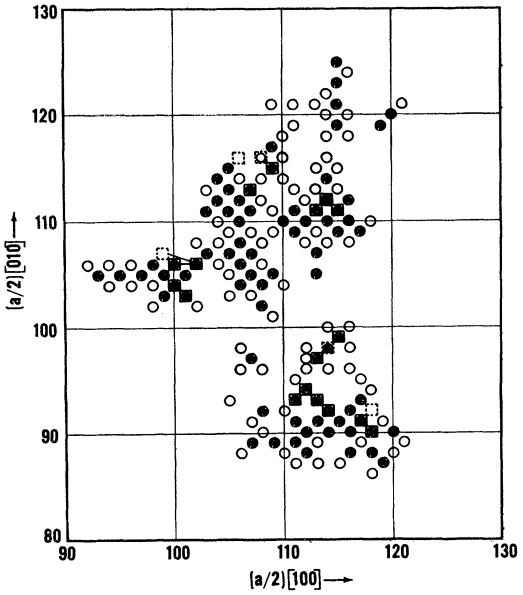

FIG. 5. Projection of the collided atom positions in a two-lattice-constant-thick slice through a 5-keV cascade collided-atom volume onto a (001) plane. The region depicted contains the centroid of the collided-atom volume and the faces of the slice are parallel to a (001) plane. Only small vacancy clusters were produced in this particular region. The unit of length is one-half the lattice constant ($\frac{1}{2}a$).

in the range $0<E_i<2E_s$ and none greater than $2E_s$. The average energy transfer to a collided atom was 3 eV. The (x,y) coordinates of each position in the collided-atom maps are common to two atoms, one with coordinate z and the other with coordinate $(z+2)$, in terms of the length unit $\frac{1}{2}a$. Usually, energy would be transferred to both of these atoms during a cascade, hence the volume of collided atoms associated with each map is $\sim 2N_c\Omega$, where N_c is the number of collided atom positions depicted (visible) and Ω is the atomic volume.

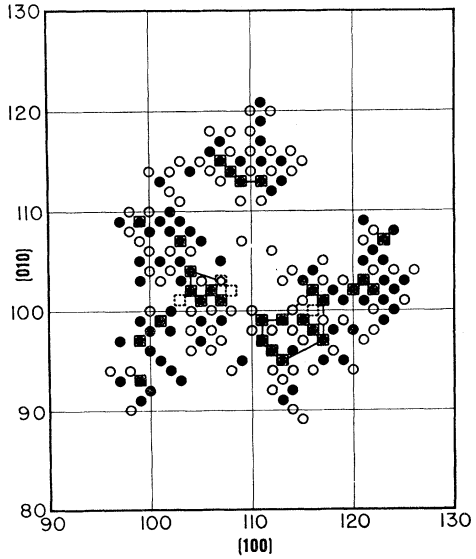

FIG. 6. Projection of the collided-atom positions in a two-lattice-constant-thick slice through a 5-keV cascade-collided-atom volume onto a (001) plane. The region contains the centroid of the collided-atom volume and the faces of the slice are parallel to a (001) plane. Large vacancy clusters were produced in this region. The unit of length is $\frac{1}{2}a$.

Each collided-atom distribution map for a (001) plane slab section through a collision cascade volume usually indicated the presence of two or more collided atom subvolumes. This feature is the result of the collided atom volume being multiply connected, i.e., possessing a Swiss-cheese structure. A three-dimensional scale model of a 5-keV cascade-collided atom volume was constructed to illustrate this multiply connected structure and the frequently observed $\langle 110\rangle$ orientation of collided-atom volumes in α-iron. A top view (along $[00\bar{1}]$) of the model appears in Fig. 8, and a view along

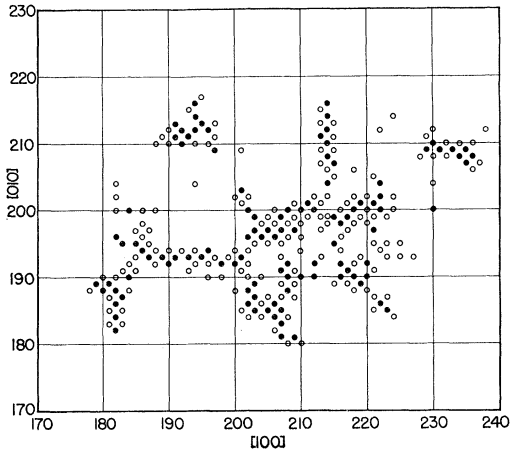

FIG. 7. Slice through the center of a 20-keV cascade collided-atom volume. The unit of length is $\frac{1}{2}a$.

$[1\bar{1}\bar{1}]$, running approximately through the centroid of the model, appears in Fig. 9. The model was constructed from wooden blocks, each of which was cut into the shape of the type of subvolumes illustrated in Figs. 5–7.

4. DISPLACEMENT-SPIKE STRUCTURE

About 3% of the collided atoms in a cascade were permanently displaced at 0°K. This collection of permanently displaced atoms and the associated vacancies constitutes a displacement spike. The positions from which atoms were permanently displaced are marked with squares in Figs. 5 and 6 to suggest direct observation of the emergence of stable vacancy configurations in the initially highly excited collided-atom volume (average energy deposition of 3 eV per atom). The associated interstitial atoms are not shown, to avoid cluttering the figure. Complete damage maps, showing both the vacancy and interstitial positions for the regions concerned in Figs. 5 and 6, appear in Figs. 10

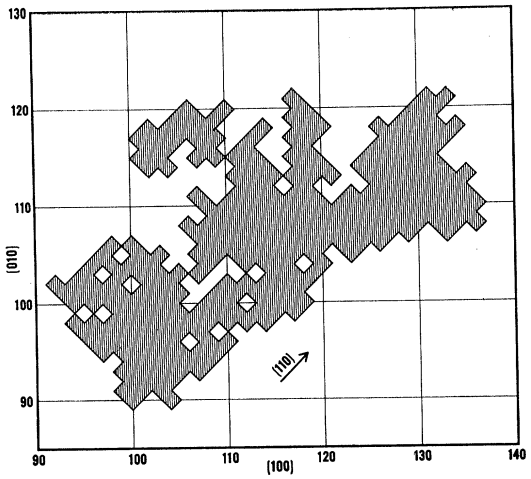

FIG. 8. Top view of a 5-keV collided-atom volume in α-iron. The unit of length is $\frac{1}{2}a$.

and 11, respectively. These maps give the projections of all vacancy (open square) and interstitial (filled circle) positions in four successive (002) planes onto a (001) plane. Defect clusters are indicated by connecting lines among the cluster members and a population number. A small open circle denotes the (x,y) position of a cluster member which lies in an atom plane above the four (002) planes concerned in the figure, and an asterisk indicates a cluster member which lies in an atom plane below the four planes concerned in the figure.

Clusters containing 10 or more vacancies will be called large clusters. It appears that clusters in this size range are particularly important. Experimental evidence indicates that large vacancy clusters dominate the contribution made by vacancies to irradiation hardening[19] and theoretical evidence (Sec. 7) indicates

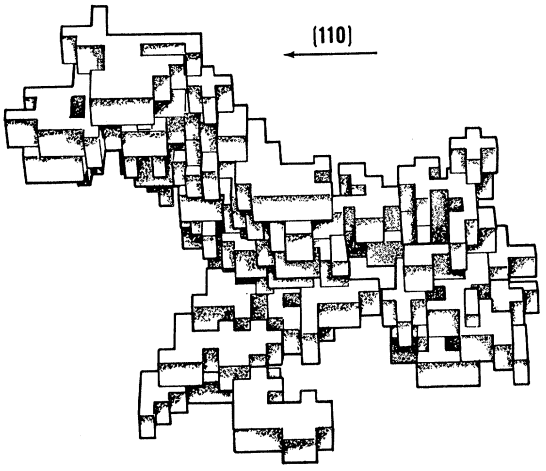

FIG. 9. View along $[1\bar{1}\bar{1}]$ of the 5-keV collided-atom volume whose top view appears in Fig. 8.

[19] G. Thomas and J. Washburn, Rev. Mod. Phys. 35, 992 (1963); J. Galligan and J. Washburn, Phil. Mag. 8, 1455 (1963).

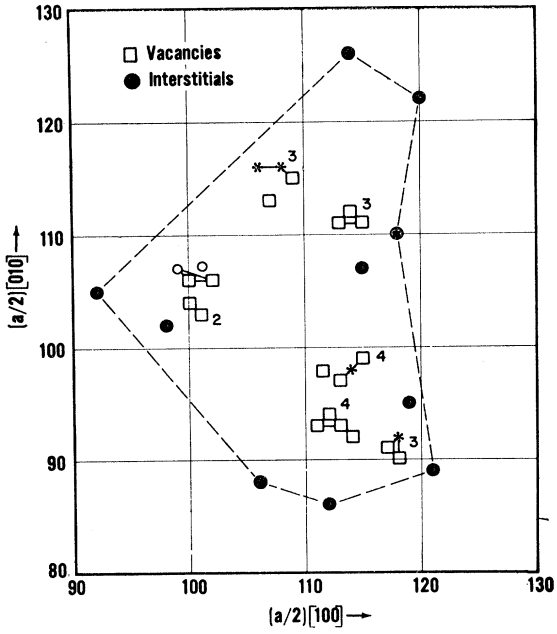

FIG. 10. Vacancy (□) and interstitial (●) development which evolved from the collided-atom distribution of Fig. 5. The unit of length is $\frac{1}{2}a$.

that displacement spikes which contain large vacancy clusters are more immune to devastation by thermal annealing than are those which do not contain large vacancy clusters. Illustrations of damage states which do not and which do contain large vacancy clusters are given by Fig. 10 and Fig. 11, respectively.

Drawings of displacement-spike models appear in Figs. 12–15. Each block in one of these models repre-

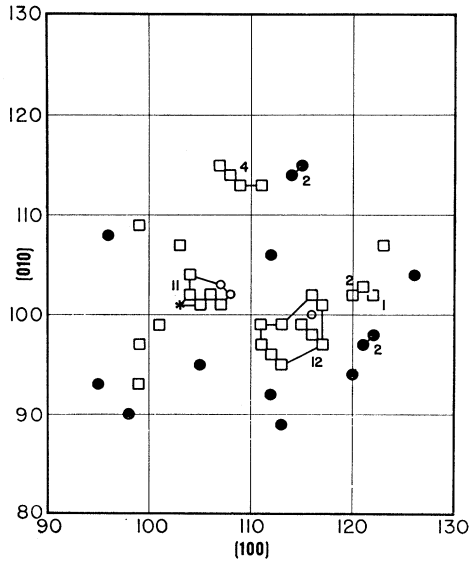

FIG. 11. Vacancy (□) and interstitial (●) deployment which evolved from the collided-atom distribution of Fig. 6. The unit of length is $\frac{1}{2}a$.

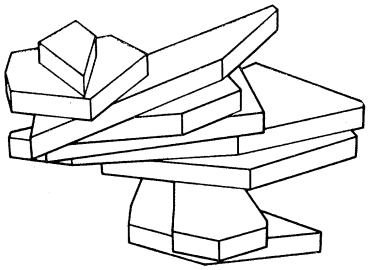

FIG. 12. Distorted lattice region associated with a 5-keV displacement spike. This particular distorted lattice region and the collided-atom volume in Fig. 8 belong to the same collision cascade.

sents the lateral extent of the damage produced in four successive (002) planes. The shape of a given block was determined by the positions of the peripheral defects in the associated damage map. The dashed boundary line in Fig. 10, for example, defines the shape of the displacement-spike model block that would be used to represent the damaged region depicted by Fig. 10. From the standpoint of irradiation effects upon mechanical properties,[20] the stacked-block, displacement-spike-volume model approximates the region of nonelastic strain associated with a displacement spike at 0°K. The elongated blocks are the result of quasichanneling. Pure channeling trajectories being much longer (10^3–10^4 Å) than a typical spike diameter (~100 Å) led to spikes which were divided into as many as four disjoint parts. Quasichanneling, usually in ⟨110⟩ directions, was sufficiently frequent to lend a significant degree of ⟨110⟩ orientation to all spikes associated with PKA energies ≥ 5 keV in α-iron and PKA energies ≥ 10 keV in tungsten. A detailed study of quasichanneling in copper is not yet finished. The characteristic displacement-spike shape which emerges from the present study is highly irregular shape which clearly cannot be closely approximated by either a spherical region or a cylindrical region with a constant cross section.

Vacancies tended to be segregated from interstitials in a displacement spike. Roughly speaking, a spike consisted of a vacancy-rich core enclosed by an interstitial-rich mantle. As a consequence, a marked imbalance existed between the vacancy and the interstitial populations within individual subregions of a spike. Specifically, in the block which contained the centroid of a spike (the central block), interstitials tended to be deployed at the periphery of the associated damage map and vacancies at the center of the map. The existence of this feature does not depend upon the vacancies being bunched together into large clusters, as is illustrated by Fig. 10 and Fig. 11. The damage distribution in Fig. 10 is for a central block which did not contain large clusters and that in Fig. 11 is for a central block which did contain large clusters. Both distributions also exhibit a local imbalance between the vacancy and the interstitial populations. In Fig. 10, for example, there are 18 vacancies and 10 interstitials. The vacancy population was usually from 1.5 to 2.5 times the interstitial population in the central block. As one proceeded away from the centroid, the relative number of interstitials increased and blocks at the ends of a spike were interstitial-rich. One would expect this type of defect deployment to favor interstitial cluster and vacancy cluster formation as a result of point defect migration. This indeed occurred in simulations of point defect annealing in a displacement spike, produced at 0°K, at a finite temperature.

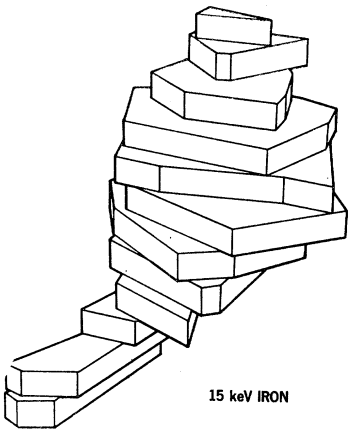

FIG. 14. Distorted lattice region associated with a 15-keV displacement spike.

The vacancy-rich core and interstitial-rich mantle result is qualitatively consistent with Brinkman's[1]

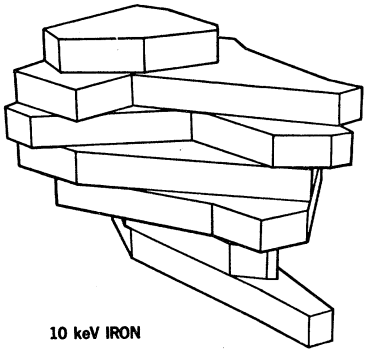

FIG. 13. Distorted lattice region associated with a 10-keV displacement spike.

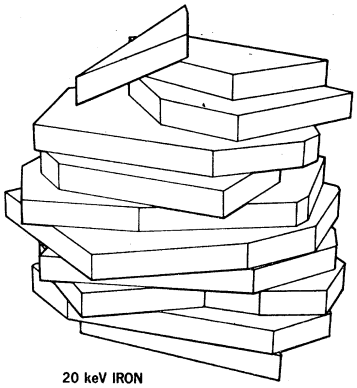

FIG. 15. Distorted lattice region associated with a 20-keV displacement spike.

[20] J. R. Beeler, Jr., J. Appl. Phys. (to be published).

concept of the general spike structure, Seeger's[21] "depleted zone" concept and the results of many-body calculations by Vineyard's group[22] for low-energy cascades (<2 keV). This general deployment also comes out of the statistical developments of Corciovei[4] and of v. Jan.[5] Vineyard,[22] for example, has discussed the fundamental physical reason for this type of defect deployment in a displacement spike. It is, essentially, that a displaced atom enjoys modes of dynamic propagation away from the position of a collision event whereas a vacancy does not. This circumstance leads to peripherally positioned interstitials. The role of replacement-collision chains in the outward propagation of displaced atoms was underestimated by our model in that the same energy of removal from a lattice site ($2E_s$) was subtracted from the energy transferred to the target atom in a replacement collision as was subtracted in an ordinary collision. One would expect that a smaller removal energy would be more appropriate to replacement collisions.

The average displacement density in a spike was independent of the initiating PKA energy over the energy range considered (0.5 to 20 keV). It also appears that the displacement density in isolated displacement spike produced at 0°K is saturated. Table I gives the average collided-atom volume as a function of the initating PKA energy in α-iron and copper, respectively, as tallied by the computer during the development of a cascade. These tallies were obtained by counting the number of subvolumes in the crystal in which at least one collision occurred for which $E_t > 2E_s$. The subvolume size was fixed at 16Ω. A clerical count of the number of collided atoms in 5 and 10 keV cascades showed that the 16Ω subvolume size was too large and caused the computer tally estimate to be about 40% larger than the true collided-atom volume. On the basis of the approximate collided-atom volume tally made by the computer, the average displacement density in α-iron was 2.3 at. % and that in copper was 1.5 at. % at 0°K for each PKA energy considered. According to

TABLE I. Computer-tally estimate of the collided-atom volume in α-iron and copper in units of atomic volume, Ω. In the case of α-iron, this estimate is about 40% larger than the true volume. The correction factor for copper is not known.

PKA energy, keV	Collided-atom volume Ω	
	Iron	Copper
0.5	300	450
1.0	550	800
2.5	1320	1750
5.0	2550	3350
10	4850	6300
15	7150	9250
20	9500	12 250

[21] A. Seeger, in *Radiation Damage in Solids* (International Atomic Energy Agency, Vienna, 1962), pp. 101–127.
[22] G. H. Vineyard, Discussions Faraday Soc. No. 31, 1 (1961).

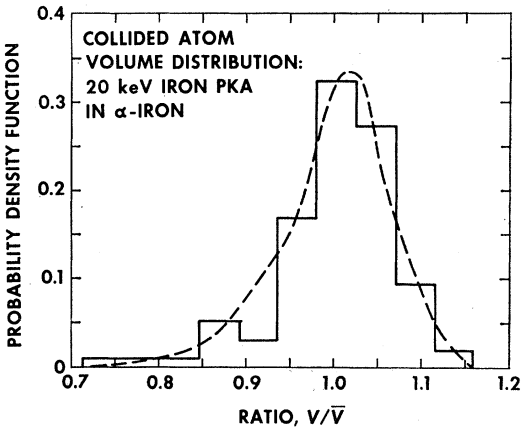

FIG. 16. The distribution of collided-atom volumes (V) about the average volume ($\bar{V}$) for 5–20-keV cascades in α-iron is typified by the above distribution for 20-keV cascades.

Lehmann,[23] the saturated displacement density should be the reciprocal of the recombination volume. If one corrects for the 40% overestimation in the computer tally approximation to the collided-atom volume, a displacement density of 3% results for α-iron. This is the saturated density magnitude associated with a 30-site recombination volume. The computer tally collided-atom-volume correction factor for copper has not yet been established.

For PKA energies in the interval 5–20 keV, the distribution of collided-atom volume magnitudes about their average did not vary significantly with PKA energy in α-iron. The volume distribution for 20 keV cascades appears in Fig. 16. Typically, about 93% of the collided-atom volumes fell within the interval $0.85\ \bar{V} - 1.10\ \bar{V}$, where $\bar{V}$ is the average collided-atom volume for the PKA energy concerned.

5. CRYSTAL-STRUCTURE EFFECTS

Displacement-production models for a structureless solid[24] predict that the average number of displacements $\nu(E)$ in a displacement spike produced at 0°K is proportional to the energy E of the initiating PKA for energies in the elastic-collision range. The most frequently used structureless solid models are the Seitz-Harrison, Snyder-Neufeld, and Kinchin-Pease models.[25] Since each of these models gives about the same number

[23] C. Lehmann (unpublished work). Dettman (Ref. 26) subsequently did a more detailed study.
[24] The structureless solid associated with a given crystalline solid is a random atomic array with the same number of atoms per unit volume as the crystalline solid.
[25] G. J. Dienes and G. H. Vineyard, *Radiation Effects in Solids* (Interscience Publishers, Inc., New York, 1957); D. S. Billington and J. H. Crawford, Jr., *Radiation Damage in Solids* (Princeton University Press, Princeton, New Jersey, 1961); D. K. Holmes, in *The Interaction of Radiation With Solids*, edited by R. Strumane, J. Nihoul, R. Gevers, and S. Amelinckx (North-Holland Publishing Company, Amsterdam, 1964); L. T. Chadderton, *Radiation Damage in Crystals* (John Wiley & Sons, Inc., New York, 1965).

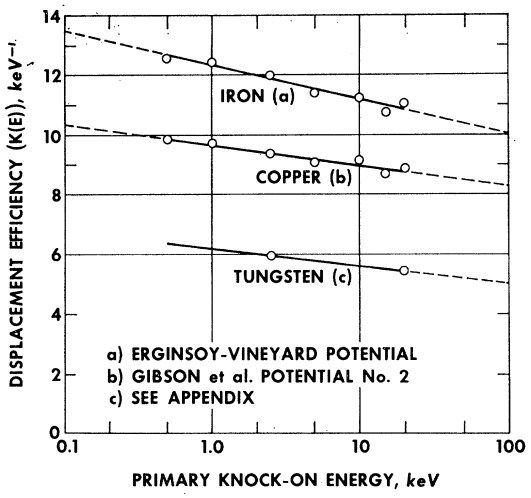

FIG. 17. Displacement efficiency $K(E)$ for α-iron, copper, and tungsten. The monotonic decrease in $K(E)$ with PKA energy E is caused almost entirely by damage production interference among cascade branches.

of displacements,[22] it will be sufficient to compare our structure-dependent results with those of any one of the structureless solid models. We have chosen to use the Kinchin-Pease model in this comparison. This model gives

$$\nu(E)=E/2E_dE>E_d, \quad (1)$$

where E_d is the displacement threshold energy. The average number of displacements per unit PKA energy, i.e., the ratio $K=\nu(E)/E$ will be called the displacement efficiency. In the Kinchin-Pease model, the displacement efficiency, $K_{kp}=1/2E_d$, is a constant. However, when crystal-structure effects are accounted for, one obtains an energy-dependent displacement efficiency

$$K(E)=\nu(E)/E, \quad (2)$$

as shown by Fig. 17 and Eqs. (3) and (4). In the case of α-iron

$$K(E)=12.33(1-0.04190\ \ln E) \quad (\alpha\text{-iron}) \quad (3)$$

and in the case of copper

$$K(E)=9.65(1-0.03150\ \ln E) \quad (\text{copper}), \quad (4)$$

where the PKA energy E is in keV. On the basis of 48 runs each for 2.5 and 20 keV in tungsten, one obtains $K_W(E)=0.49K_{Fe}(E)$ where K_W and K_{Fe} are the displacement efficiencies for tungsten and α-iron, respectively.

The monotonic decrease in the displacement efficiency with increasing PKA energy was caused principally by two crystal-structure effects. One of these was damage production interference among different parts of a cascade and the other was long-range channeling. Interference was manifested largely by the recombination of an interstitial from one collision event and a vacancy from another collision event along close-packed lines of atoms. Leibfried[26] refers to this interference process as a thermal annealing in his treatment of recombination events during displacement-spike formation. Interference was by far the dominant effect in α-iron and tungsten, and completely determined the energy dependence of the displacement efficiency in copper. Although the effect of long-range channeling was always to reduce damage production, quasichanneling would enhance the production of stable damage under certain circumstances.

A. Interference Effects

According to Erginsoy *et al.*,[7] the Frenkel pair recombination region for α-iron at 0°K is that pictured in Fig. 4. An interstitial (split configuration) at any one of the 24 noncentral open-circle positions on the ⟨111⟩ lines or any one of the 6 hatched-circle positions on the ⟨100⟩ lines will recombine with a vacancy at the central open-circle position without thermal activation. A comparable region (42 sites), was obtained by Gibson *et al.*[9] for copper. In copper, the greatest recombination range, again three interatomic distances, is along ⟨110⟩ lines. As mentioned in Sec. 2, these recombination regions were used in the present study to determine the stable-damage state at 0°K.

The influence of the recombination region is partially accounted for in the Kinchin-Pease model through the displacement threshold energy E_d. By definition E_d is the average minimum energy transfer required to produce a permanently displaced atom, i.e., a stable Frenkel pair. As such, E_d pertains to the average outcome of *isolated* collision events in an otherwise perfect crystal, and is determined experimentally via low-beam-intensity electron-bombardment experiments. However, the collided-atom distribution maps of this study and the trajectory maps from the many-body calculations of Gibson *et al.*, and Erginsoy *et al.*, for example, clearly show that a displacement event in a collision cascade is not an isolated event, and that the state of the surrounding crystal region may be far from perfect. In the case of a collision cascade, the question of whether a nascent Frenkel pair will survive in the current damage state cannot be answered solely in terms of a simple displacement threshold energy or even in terms of a direction-dependent threshold energy. The immediate survival of the pair depends upon the distribution of existing defects, and the persistence of either member upon the distribution of defects subsequently created. Different branches of a cascade can interfere with one another in the process of defect production in addition to interference between successive collision events in the same collision branch. In this sense, the number of displacements in a displacement spike is equal to the product N_eq_r, where N_e is the number of atoms ejected

[26] G. Leibfried, Atomic Energy Research Establishment, Harwell, Report No. AERE-R4694 (unpublished); K. Dettmann, Phys. Status Solidi **10**, 269 (1965).

TABLE II. Number of collisions $N(E_t>E':E)$ for which $E_t>E'$ in α-iron. E is the PKA energy.

E, keV	$N(E_t>E':E)$ $E'=8$ eV	$E'=25$ eV	$E'=32$ eV	$N=E/2E'$ [a]
1	66.7	25.5	19	20
5	330	127	96	100
10	···	255	···	200

[a] For $E_d=25$ eV.

from a normal lattice site and q_r is the probability that an ejected atom will not recombine with a vacancy. It will now be shown that in the cascade simulations, N_e was proportional to the energy of the initiating PKA and that q_r was a function of PKA energy, crystal structure, and irradiation temperature. The temperature dependence of q_r was determined in part.

In each metal, $K(E)$ was smaller than the Kinchin-Pease displacement efficiency at all energies in addition to being a monotonically decreasing function of the PKA energy. This behavior is especially interesting in view of the fact that given an energy value $E'<50$ eV, the number of collisions $N(E_t>E':E)$ for which $E_t>E'$, in a cascade initiated by a PKA with energy E, was proportional to E. This type of behavior is exactly that assumed in structureless solid models, the Kinchin-Pease model in particular. Table II gives $N(E_t>E':E)$ in α-iron for $E'=8$, 25, and 32 eV. The 8-eV value corresponds to the minimum energy transfer for which an atom was ejected in the present study and $E_d=25$ eV is a value commonly used in estimating damage production in either iron or copper using a structureless solid model. In all instances, the magnitude of $N(E_t>E':E)$, computed on the basis of the Erginsoy-Vineyard potential, exceeded that given by the Kinchin-Pease formula, i.e., $E/2E_d$ with $E_d=E'$, which was derived on the basis of hard-sphere collisions. The right-hand column in Table II gives the Kinchin-Pease result for $E_d=E'=25$ eV for comparison with $N(E_t>E'=25$ eV$:E)$ in the second column. The same type of results were obtained for copper. Table II shows (1) The observed inequality $K(E)<K_{KP}$ cannot be explained on the basis that a smaller number of collisions for which $E_t>E_d$ occurs, when the Erginsoy-Vineyard potential is used, than is predicted by the Kinchin-Pease model. In fact, $N(E_t>E':E)\simeq 1.2E/2E'$ for $E'\geq 25$ eV. (2) The slope of $N(E_t>E':E)$ is constant, hence the observed monotonic decrease in $K(E)$ with energy cannot be caused by a change in the slope of $N(E_t>E':E)$.

Because $N(E_t>E':E)$ was proportional to E, as in the theory for a structureless solid, only direct interstitial-vacancy recombination during cascade development and channeling remain as possible mechanisms for causing a monotonic decrease in $K(E)$ with energy, in our model, at 0°K. A comparison of the number of ejected atoms and the number of ultimately stable displacements showed directly that the relative number of recombination events increased with PKA energy and accounted for 97% of the variation in $K(E)$ in α-iron and tungsten. All of the energy dependence of $K(E)$ in copper appears to be caused by interference effects.

The type of recombination discussed above is called direct recombination. There also exists the possibility of indirect recombination at 0°K which is induced by localized lattice vibrations which have been excited by the cascade.[27] In these instances an interstitial can be induced to recombine with a vacancy even though it lies completely outside the 0°K instability region for Frenkel pairs in an unexcited lattice. This indirect recombination process cannot be properly described within the framework of the binary collision model. However, it can and has been treated in a dynamic, many-body calculation by Erginsoy *et al.*[8] In this respect, if we use the computed value of $\nu(E)$ from the cascade simulations and the Kinchin-Pease equation to define an effective displacement threshold energy, $\nu(E)=E/2E_{\text{eff}}$, we find $E_{\text{eff}}\simeq 42$ eV for $1<E<2$ keV on the basis of direct recombination alone. Erginsoy *et al.*, obtain a larger value $E_{\text{eff}}=50$–55 eV in their dynamic calculations. This suggests that indirect recombination exerts a significant influence at 0°K.

The effective displacement energies predicted by a binary collision model with an appended many-body recombination region scheme and those given by a dynamic, many-body model are only about a factor of 2–3 larger than that which has been used for some time in structureless-solid theory.[25] This factor by itself does not explain the order of magnitude differences which exist between the Kinchin-Pease result and measured defect production at finite temperatures. Lück and Sizmann,[28] for example, find that a recombination region of $\sim 150\ \Omega$ is required to explain damage-production results for fcc metals at finite temperatures (10–90°K). The possible growth of the region for interstitial-vacancy recombination by correlated motion with increasing temperature immediately suggests itself.

An attempt was made to describe the increase in the recombination region volume with increasing temperature in α-iron using Johnson's program[29] for defect configuration calculations to compute the activation energies involved. Frenkel pairs composed of interstitials at third- and fourth-neighbor positions, relative to the vacancy, and at positions along [111] separated from the vacancy by 4–8 interactomic distances were considered. All of the positions lie outside the Erginsoy-Vineyard recombination region for 0°K. Runs were also made for vacancy migration along [111] toward the interstitial, a process which also can induce

[27] G. Burger, H. Meissner, and W. Schilling, Phys. Status Solidi 4, 267 (1964); 4, 281 (1964).
[28] G. Lück and R. Sizmann, Phys. Status Solidi 5, 683 (1964).
[29] R. A. Johnson, Phys. Rev. 134, A1329 (1964).

TABLE III. Recombination activation energy $E_r(i)$ for interstitial motion toward a vacancy along a [111] atom line in α-iron for four initial separation distances along [111]. d_1 is the interatomic distance and $E_m(i)=0.33$ eV is the interstitial migration energy in a perfect crystal computed by Johnson.[a]

Initial separation	$E_r(i)$, eV	$E_r(i)/E_m(i)$
$4d_1$	0.06	0.18
$5d_1$	0.21	0.64
$6d_1$	0.31	0.94
$7d_1$	0.33	1.0

[a] Reference 29.

interstitial-vacancy recombination. The migration energy results for the [111] positions are given in Tables III and IV. In dynamic calculations performed with the GRAPE program,[7,8] also a Brookhaven code, interstitials excited to 0.33 eV recombined with the vacancy within 10^{-12} sec when their initial positions were a fourth-neighbor site, relative to the vacancy, and a site four interatomic distances from the vacancy along [111] (17th neighbors). An interstitial excited to 0.33 eV at either a third-neighbor site or a site five interatomic distances from the vacancy along [111] did not recombine with the vacancy within 10^{-12} sec. Furthermore, no recombination events were observed for interstitials excited to 0.16 eV at 4th- and 17th-neighbor sites. According to Johnson's calculations[29] the interstitial migration energy in α-iron is 0.33 eV, and Lucasson and Walker[30] have shown that interstitials move freely in α-iron at 120°K. This suggests that 4th- and 17th-neighbor interstitials should be sufficiently excited at 120°K to recombine with the reference vacancy. On this basis, the recombination region at120°K should encompass, at least, 4th and 17th neighbor sites in addition to those included in the 0°K recombination region. There are 32 such additional sites, hence the 120°K recombination region ($\geq$62 sites) should be at least twice as large as the 0°K recombination region. On the basis of the calculations done thus far, it is conceivable that the correlation motion recombination volume could grow to include $\sim$100 sites at higher temperatures. A detailed account of these calculations will be given in a later article.

TABLE IV. Recombination activation energy $E_r(v)$ for vacancy motion toward an interstitial along a [111] atom line in α-iron for three initial separation distances along [111]. d_1 is the interatomic distance and $E_m(v)=0.68$ eV is the vacancy migration energy in a perfect crystal computed by Johnson.[a]

Initial separation	$E_r(v)$, eV	$E_r(v)/E_m(v)$
$4d_1$	0.16	0.24
$5d_1$	0.60	0.88
$6d_1$	0.68	1.0

[a] Reference 29.

As is well known,[25] the number of displaced atoms indicated by electrical resistivity change measurements is about an order of magnitude smaller than that predicted by the structureless-solid models. In this respect, the above results suggest that the neglect of damage production interference among different parts of a cascade and the temperature dependence of the recombination volume are the principal deficiences of the structureless solid models with respect to predicting the number of displaced atoms. If one takes a factor of 2.5 reduction, due to crystal-structure effects, and an additional factor of 2 reduction, due to growth of the recombination volume, a combined reduction factor of 5 results for irradiation at 120°K *prior* to any thermal annealing via interstitial movement. If the recombination volume can indeed grow to $\sim$100 sites at higher temperatures, a factor of $>$8 reduction could occur without the advent of thermal annealing via interstitial movement. In this context, of course, the term 'thermal annealing via interstitial movement' pertains to long-range interstitial migration characterized by the perfect-crystal activation energy for interstitial migration.

In addition to the above purely crystal-property aspects of the problem, there is the possibility that the measured electrical resistance change is not properly interpreted as a measure of displaced atom content in a displacement spike. Corciovei and Babcenco[31] have computed the electrical resistivity change produced by an isolated displacement spike. They show that the resistivity change due to a displacement spike, considered as an entity of correlated interstitials and vacancies, does not reduce to a simple sum of the contributions of independent interstitial-vacancy pairs; rather, it is smaller than the resistivity-change sum over independent pairs. They give numerical results for a 200-eV cascade in copper. In this instance, the spike resistivity was about $\frac{1}{3}$ that of the sum of the "individual" defect resistivities.

A combination of the considerations of Corciovei and Babcenco with those coming from crystal-structure-sensitive damage calculations can account for as much as a factor of 24 difference between the damage production predicted by a structureless-solid model and that indicated by electrical-resistivity measurements prior to thermal annealing. During thermal annealing, however, the loss of point defects will progressively weaken the initial correlation between interstitial and vacancy positions on which the result of Corciovei and Babcenco is based. Hence, the displacement spike resistivity contribution must tend toward that given by a simple sum of contributions by independent defects of annealing proceeds.[32]

[30] P. G. Lucasson and R. M. Walker, Phys. Rev. **127**, 485 (1962).

[31] A. Corciovei and A. Babcenco, Phys. Status Solidi **4**, 587 (1964).

[32] The author is indebted to T. O. Ziebold for pointing out this circumstance.

B. Channeling Effects

In an earlier calculation for α-iron, based on the Bohr potential collision diameter and the hard-sphere scattering model, long-range channeling appeared to be the dominant effect in producing an energy dependent displacement efficiency.[33] When the Erginsoy-Vineyard potential is used, however, only a 3% reduction in displacement production can be ascribed to long-range channeling at 0°K. This fraction was determined directly by comparing the average number of displacements produced by cascades in which long-range channeling occurred with that in cascades in which long-range channeling did not occur. The ⟨110⟩ direction was the most frequently adopted self-channeling[34] direction in α-iron. This is of interest because the penetration of externally injected atoms into α-iron was larger by far along ⟨100⟩ channels than along ⟨110⟩ channels. The preference of ⟨110⟩ direction for self-channeling in α-iron is possibly explained by the results shown in Fig. 18. Note that the greatest penetration occurred when an iron atom was started down the center of a ⟨100⟩ channel. However, when started off-center down a ⟨100⟩ channel, the channeling range dropped off precipitously. In contrast, although the maximum ⟨110⟩ channeling range is only about $\frac{1}{3}$ that along ⟨100⟩, the particular starting position within the core of the ⟨110⟩ channel did not much affect the channeling range at 5 keV and exerted virtually no effect at 10 keV. It would seem that this insensitivity of the ⟨110⟩ channeling range on starting position would favor ⟨110⟩ as the predominant directions for self-channeling. According to Ralph,[35] field ion microscope examinations of neutron irradiated α-iron and tungsten indicate a strong preference for long-range energetic atom motion along⟨110⟩ directions rather than along ⟨100⟩ directions.

Table V gives the fraction of all PKA ranges greater than a given distance at each PKA energy in α-iron and copper. Although definite statements can be made about the relative frequency of quasichanneling and long-range channeling in these metals, a detailed range analysis is not possible because only 96 cascades were run at each energy. A lower limit on the range length for quasichanneling was estimated by assuming a trial value R_0 for this limit and then comparing the average range over $0<R<R_0$ versus PKA energy with that computed by Oen *et al.*,[36] for a structureless solid. The resulting curve was more similar to that of Oen *et al.*, for $R_0=100$ Å than for larger or smaller R_0 values taken at 20 Å intervals. Because of long-range channeling, the average over all ranges rose much more rapidly with energy than did the Oen *et al.*, curve, above 5 keV. Quasichanneling probabilities in the range 0.08 to 0.24 are obtained for PKA energies $E\geq 5$ keV when the entries in Table V for $R\geq 1000$ Å (long-range channeling) are subtracted from those for $R\geq 100$ Å.

TABLE V. Fraction of PKA ranges greater than a given distance in the channeling-range region for α-iron and copper.

Range, Å	PKA energy, keV 2.5	5	10	15	20
		α-Iron			
$R\geq 100$	0.052	0.125	0.137	0.260	0.274
$R\geq 150$	0.042	0.094	0.095	0.167	0.095
$R\geq 200$	0.031	0.083	0.063	0.156	0.042
$R\geq 300$	0.010	0.073	0.063	0.125	0.032
$R\geq 500$	0	0.073	0.053	0.115	0.032
$R\geq 1000$	0	0.010	0.053	0.083	0.032
		Copper			
$R\geq 100$		0.032	0.021	0.156	0.250
$R\geq 150$		0.010	0.010	0.052	0.062
$R\geq 200$		0	0	0.010	0.021
$R\geq 300$		0	0	0.010	0.010
$R\geq 500$		0	0	0.010	0
$R\geq 1000$		0	0	0	0

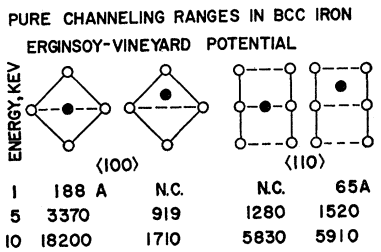

FIG. 18. Effect of starting position on the channeling range along ⟨100⟩ and ⟨110⟩ directions in α-iron. The notation N.C. means "no channeling." Note that the ⟨110⟩ channeling range is much less sensitive to the starting position than is the ⟨100⟩ channeling range.

Long-range channeling of PKA in α-iron started at an energy between 2–5 keV and persisted through 20 keV. No long-range channeling occurred in copper. Harrison *et al.* also obtained this result in their n-body calculation. Note that the probability for PKA channeling in α-iron appears to peak in the vicinity of 15 keV. Over the 5–20-keV energy interval, the average probability for PKA long-range channeling was 0.04; for energies above 10 keV it was 0.06. This is the probability that a given PKA will execute a long-range channeling event sometime during its history. However, in most instances, an atom which executed such a trajectory expended from 20–50% of its energy prior to achieving the long-range channeling trajectory and this trajectory was usually disrupted while the atom energy was in the interval between 2 and 1 keV. Hence, it was possible for a 20-keV PKA to exhibit long-range channeling and yet expend as much as 60% of its energy in

[33] J. R. Beeler, Jr., and D. G. Besco, Phys. Rev. 134, A530 (1964).

[34] The term self-channeling applies to an atom which has been ejected from a normal atom site in a crystal and then adopts a channeled trajectory during some part of its history.

[35] B. Ralph (private communication).

[36] O. S. Oen, D. K. Holmes, and M. T. Robinson, J. Appl. Phys. 34, 302 (1963).

normal damage production. Similarly, a 5-keV PKA could exhibit long-range channeling and expend 70% of its energy in normal damage production. Even though the average probability per PKA for long-range channeling was sizeable (0.04–0.06), the typical prolonged introductory phase indicates that the channeling probability per collision is small. The number of collisions in the introductory phase ranged from the order of 10^1 to 10^2. This indicates that the channeling probability per collision ranges from 5×10^{-3} to 5×10^{-4}.

The choice of 1000 Å as the lower limit for long-range channeling was somewhat arbitrary. It was chosen principally to ensure that the channeling events thus defined would be almost completely independent of events occurring in any other branch of the cascade. Setting the lower limit at 1000 Å gives a length which is 5–10 times larger than the diameter of a typical cascade. This ensures independence with respect to damage produced by other cascade branches. Only very nicely focused trajectories extend further than about 1000 Å. In these instances, the energy transfer per collision is usually less than 1 eV and rarely exceeds 3 eV. As a consequence, it is virtually impossible for two successive ejection events along the trajectory to occur sufficiently close to interfere with one another. Under these conditions, one can definitely ascribe a decrease in displacement efficiency as being caused solely by channeling. Any interstitial-vacancy recombination concerns only one ejected atom and the particular vacancy at the site from which it was ejected.

In the case of quasichanneling, interactions among different Frenkel pairs may occur and any damage reduction observed cannot be ascribed solely to the existence of channeling. In fact, the occurrence of quasichanneling can enhance the production of stable damage configurations under certain conditions: This enhancement occurs when the quasichanneled atom moves outward from the center of the cascade and its energy is such that the separation distance between successive sites from which it has displaced atoms is greater than the diameter of the recombination region. In this instance, the damage reduction which would ordinarily arise as a result of interactions between Frenkel pairs is circumvented and the probability against recombination q_r is increased as a consequence. One can conjecture that there may be instances in which the diameter of the recombination region could be so large relative to the average separation distance between successively ejected atoms that the major portion of any stable damage production would be due to quasichanneled atoms. In this respect, irradiation at high temperatures suggests itself as such an instance.

C. Probability against Recombination at 0°K

Table VI describes the average probability $\bar{q}_r$ against recombination in tungsten, α-iron, and copper at energies in the range 5–20 keV. An estimate of the probability against direct recombination q_r' is given by the ratio N_d'/N_e', where N_d' is the average number of displaced atoms and N_e' the average number of ejected atoms per keV of PKA energy. The average is taken over the kinetic energy and initial direction of an ejected atom. A comparison of the effective displacement energy (42 eV) for 1–2-keV PKA in α-iron given by the present study with that (50–55 eV) given by the dynamic, many-body calculations of Erginsoy *et al.*,[8] for the same energy range, gives $q_r\simeq0.8q_r'$, where q_r is the probability against both direct and indirect recombination. If the density of ejected atoms were the same in each instance, the q_r' for two different metals would stand in the same proportion as do the reciprocals of their recombination volumes. The probabilities for α-iron and copper do stand approximately in this proportion. Since $V_R(\mathrm{W})=V_R(\mathrm{Fe})$, where V_R is the recombination volume in units of atomic volumes, the inequality $q_r'(\mathrm{W})>q_r'(\mathrm{Fe})$ suggests that the density of ejected atoms in tungsten cascades is smaller than that in α-iron cascades.

TABLE VI. Average probability against recombination, q_r, over the energy range 5–20 keV. q_r' is the probability against direct recombination, N_e' is the average number of ejected atoms per keV of PKA energy, E_s is the sublimation energy, and V_R is the recombination volume at 0°K in units of Ω, the atomic volume.

Metal	$2E_s$	N_e'	q_r'	q_r	V_R
W	18	29	0.19	0.15	30
α-Fe	8	66	0.16	0.13	30
Cu	7	74	0.12	0.10	42

6. DEFECT-CLUSTER SIZE DISTRIBUTION

Following Makin *et al.*,[37] an aggregate of vacancies or of interstitials formed directly during a collision cascade will be called an embryo cluster. Embryo clusters are not independent entities in at least two respects: (1) Their formation depends in part upon the superposition of aggregates produced by different branches of a cascade; (2) The field of relaxed atoms about each embryo cluster in a displacement spike overlaps that of at least one other defect. Characteristic (1) appears to limit the aggregate content of a few tens of vacancies and less than five interstitials. Characteristic (2) causes atom transport during the simulated initial annealing stage to be dominated by "snap-in" recombination processes along ⟨111⟩ directions.

Embryo vacancy clusters containing as many as 21 vacancies were observed in α-iron and copper but the largest embryo interstitial cluster observed was a tri-interstitial in α-iron and tungsten, and a tetrainterstitial in copper. The symbols v_n and i_n will be used to denote an n-vacancy and an n-interstitial cluster, re-

[37] M. J. Makin, A. D. Whapham, and F. J. Minter, Phil. Mag. 7, 285 (1962).

spectively. A vacancy cluster in α-iron was taken to be any collection of vacancies deployed such that no member of the collection was positioned more than one lattice constant from at least one other member. A vacancy cluster in copper was taken to be any collection of vacancies deployed such that no member of the collection was positioned more than one nearest-neighbor distance from at least one other member. Interstitial clusters were defined in the same manner as were the vacancy clusters in each metal. These definitions were based on Johnson's calculations on defect configurations in copper[38] and α-iron[29] and cluster calculations made at our laboratory[39] using Johnson's computer program.

A. Vacancy Clusters

The fraction of the total number of vacancies contained in embryo vacancy clusters of each individual size is listed in Table VII for α-iron and in Table VIII for copper. The *relative* frequency with which each of the possible cluster shapes for a given v_n occurred was not that given by a random superposition of defects. This indicates that the superposition process mentioned in the first paragraph of this section does not completely negate the influence of the structure of each successive collision chain on the structure of the aggregate formed during the superposition process. No striking change occurred in the distribution of vacancy cluster sizes as a function of the initiating PKA energy. Indeed, the relative numbers of v_1, v_2, and v_3 configurations, averaged over all spikes for a given energy, were remarkably constant. These configurations collectively contain about 68% of the vacancies produced in α-iron and about 73% of those produced in copper. It was possible, at least in the case of α-iron, to distinguish between a low-energy (0.5–2.5 keV) and a high-energy (5–20 keV) size distribution for the clusters containing more than three vacancies by averaging the data in Table VII. Low-energy and high-energy distributions of this type are given in Table IX for α-iron and also for copper. In the case of α-iron, the relative number of clusters with sizes v_4 to v_9 decreases by about 12% as one goes from the low-energy to the high-energy distribution. Only a 4% decrease in the relative population of these clusters occurs in copper. In contrast, the large cluster relative population in the high-energy distribution for copper is 50% larger than the large cluster relative population in the low-energy distribution. Large clusters exist only in the high-energy distribution in α-iron. This behavior parallels the type of change in the vacancy-cluster size distribution which occurs when a sequence of collision cascades is run through the same region in a crystal.[3] It is caused by the higher degree of

TABLE VII. Fraction of the total number of vacancies contained in n-vacancy embryo clusters for displacement spikes in α-iron.

Cluster size (n)	PKA energy, keV 0.5	1	2.5	5	10	15	20
1	0.352	0.326	0.328	0.336	0.350	0.356	0.351
2	0.208	0.194	0.211	0.191	0.202	0.193	0.203
3	0.129	0.125	0.125	0.145	0.135	0.129	0.131
4–6	0.254	0.243	0.196	0.244	0.202	0.196	0.203
7–9	0.058	0.111	0.091	0.057	0.072	0.079	0.070
≥10	0	0	<0.04[a]	0.055	0.038	0.046	0.042

[a] This fraction lies in the range 0.02–0.04.

TABLE VIII. Fraction of the total number of vacancies contained in n-vacancy embryo clusters for displacement spikes in copper.

n	PKA energy, keV 0.5	1	2.5	5	10	15	20
1	0.377	0.362	0.350	0.372	0.378	0.384	0.392
2	0.200	0.225	0.222	0.213	0.200	0.214	0.218
3	0.160	0.129	0.129	0.136	0.135	0.139	0.131
4–6	0.213	0.200	0.205	0.180	0.203	0.185	0.180
7–9	0.030	0.070	0.059	0.068	0.053	0.048	0.052
≥10	0.021	0.011	0.034	0.028	0.031	0.031	0.026

TABLE IX. Fraction of vacancies in n-vacancy clusters for low-energy and high-energy displacement spikes in copper and α-iron.

		n 1	2	3	4–6	7–9	≥10
Cu:	0.5–1 keV	0.37	0.21	0.14	0.21	0.05	0.02
	2.5–20 keV	0.38	0.21	0.14	0.19	0.06	0.03
	$\bar{n}$	1	2	3	4.6	7.7	12.3
Fe:	0.5–2.5 keV	0.34	0.20	0.13	0.23	0.10	···
	5–20 keV	0.35	0.20	0.13	0.21	0.07	0.04
	$\bar{n}$	1	2	3	4.7	7.7	12.2

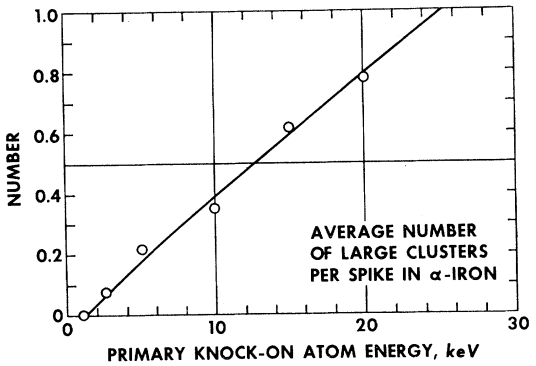

FIG. 19. Average number of large vacancy embryo clusters in an α-iron displacement spike. A large cluster is one containing 10 or more vacancies.

[38] R. A. Johnson and E. Brown, Phys. Rev. **127**, 446 (1962).
[39] J. R. Beeler, Jr., Bull. Am. Phys. Soc. **11**, 272 (1966).

cascade branch interference in a high-energy cascade relative to that in a low-energy cascade. The $\bar{n}$ values given in Table IX are the average number of vacancies per cluster in the indicated cluster groups.

The probability of finding at least one vacancy cluster containing n or more vacancies in an α-iron displacement spike is given by Table X. Bold-face type

TABLE X. Probability for at least one embryo vacancy cluster containing $\geq n$ vacancies in an α-iron displacement spike.

PKA energy, keV	n = 1	2	3	4	5	6	7	8	9	10
0.5	1.0	**0.95**	**0.62**	0.38	0.25	0.12	0.05	0	0	0
1	1.0	1.0	**0.92**	**0.69**	0.46	0.30	0.18	0.10	0.04	0
2.5	1.0	1.0	1.0	**0.92**	**0.77**	**0.60**	0.45	0.29	0.18	0.06
5	1.0	1.0	1.0	**0.98**	**0.92**	**0.73**	**0.55**	0.38	0.27	0.23
10	1.0	1.0	1.0	1.0	1.0	**0.94**	**0.80**	**0.64**	**0.50**	0.32
15	1.0	1.0	1.0	1.0	1.0	**0.98**	**0.95**	**0.82**	**0.65**	0.50
20	1.0	1.0	1.0	1.0	1.0	**0.99**	**0.95**	**0.87**	**0.72**	**0.57**

denotes the probability entries which exceed one-half but are less than unity. This division emphasizes the greater variety of cluster sizes which exists in a given high-energy spike relative to that one would find in a given low-energy spike. The average number of large clusters per spike is plotted in Fig. 19 for α-iron. An average of one large cluster per spike is attained when the PKA energy reaches $\sim$25 keV. Table XI gives the

TABLE XI. Probability for exactly n large embryo vacancy clusters occurring in an α-iron displacement spike.

n	PKA energy, keV 1	2.5	5	10	15	20
1	0	0.06	0.21	0.27	0.39	0.40
2	0	0	0.01	0.04	0.08	0.13
3	0	0	0.11	0.	0.02	0.04
≥ 4	0	0	0	0	0	0

probability of finding exactly one, two, or three large clusters per spike. The probability that a given spike contains at least one large cluster extrapolates to unity at 35 keV. Because it appears that only large vacancy-cluster configurations should survive thermal annealing in a pure metal, these large-cluster data should be pertinent to the interpretation of defect-annealing behavior after low-temperature neutron irradiation. This is discussed elsewhere in relation to irradiation hardening in α-iron.[20]

B. Interstitial Clusters

Interstitial atoms appeared almost exclusively in i_1 and i_2 configurations. At least 99% of the interstitial atoms produced in copper appeared in these configurations. In α-iron at least 99.5% of the interstitial atoms were in i_1 and i_2 configurations. The embryo interstitial cluster size distributions for α-iron and copper are given in Tables XII and XIII, respectively.

TABLE XII. Fraction of all interstitials in n-interstitial embryo clusters for displacement spikes in α-iron.

n	PKA energy, keV 0.5	1	2.5	5	10	15	20
1	0.98	0.97	0.96	0.95	0.94	0.94	0.94
2	0.02	0.03	0.04	0.05	0.06	0.06	0.06
3	0	0	0.002	0.001	0.003	0.003	0.003

TABLE XIII. Fraction of all interstitials in n-interstitial embryo clusters for displacement spikes in copper.

n	PKA energy, keV 0.5	1	2.5	5	10	15	20
1	0.97	0.95	0.93	0.92	0.90	0.90	0.91
2	0.03	0.05	0.07	0.07	0.09	0.09	0.08
3	0	0.003	0	0.01	0.01	0.01	0.01
4	0	0	0	0	<0.001	<0.001	<0.001

7. ANNEALING

Eyre's[40] electron-microscope study of neutron-irradiation damage in α-iron indicates that vacancies remain immobile in this metal below 250°C. The work of Lucasson and Walker[29] shows that iron interstitials, however, are mobile at −153°C. This being the case, one would expect that a useful approximation to the type of displacement spike produced at a finite-irradiation temperature T in the range $-153<T<250$°C could be obtained by simulating interstitial migration in a spike produced at 0°K. This expectation is supported by Schilling's[41] experimental results for copper.

Exploratory annealing simultations were done for 1 keV and 2.5 keV spikes in α-iron. Starting with a displacement spike produced at 0°K, each extant mono-interstitial and di-interstitial was moved about in a *symmetric* random walk on the α-iron lattice. Whenever an interstitial moved into the recombination region about a vacancy the two defects were immediately annihilated. When an interstitial moved to within a second-neighbor distance of another interstitial they were assumed to become bound together. Simultaneous random walks by all mobile interstitial configurations were executed by selecting a mobile configuration at random and *without replacement* from the extant damage distribution. The selected defect was, in general,

[40] B. L. Eyre and A. F. Bartlett, Phil. Mag. **12**, 261 (1965).
[41] W. F. Schilling (private communication).

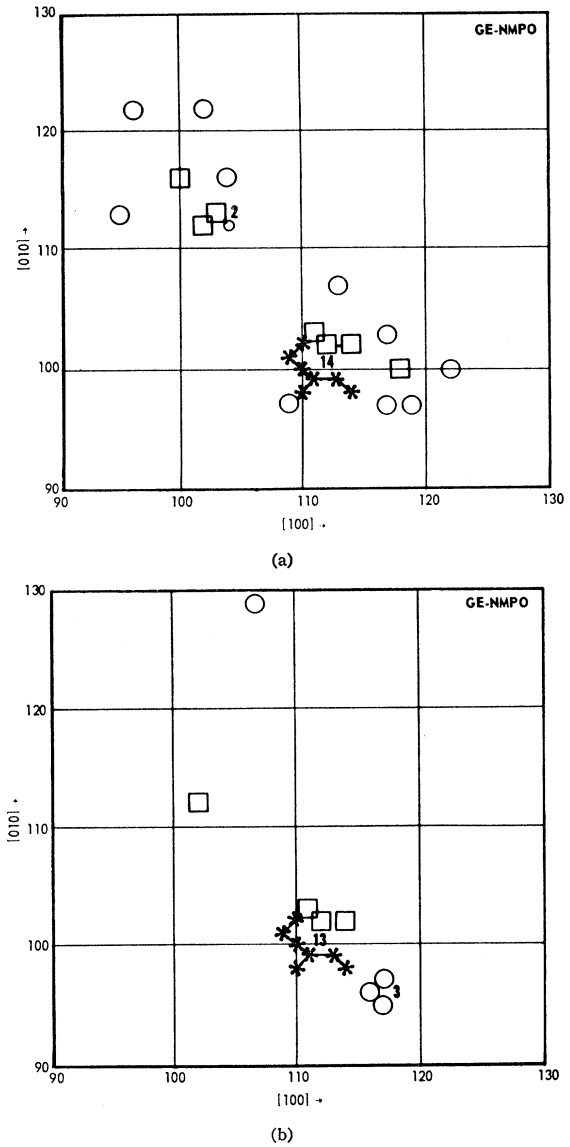

FIG. 20. (a) Vacancies (□) and interstitials (○) in a slice from a displacement spike produced and retained at 0°K. (b) Vacancies and interstitials in the same slice at $t=37\tau$ (τ=interstitial jump time) after an up-quench from 0°K to a temperature at which interstitials migrate but not vacancies. Note the removal of small clusters and the survival of the large cluster. Nearly all remaining defects are cluster members.

allowed to do one of three things: (1) jump to a new site, (2) dissociate, or (3) remain with both position and configuration unchanged. Each mobile configuration was considered in this way exactly once during each time interval τ. The principal condition on τ was that it be sufficiently small that the probability for any defect to execute two successive events within time τ would be negligible. In practice τ was set equal to the average jump time for the defect with the largest jump frequency. The full generality of the computer program for annealing was not utilized in that the same jump time (τ) was assigned to both mono- and di-interstitials and the di-interstitial dissociation probability was assumed to be zero.

The simulated initial annealing process was very fast because of the saturated displacement density in a primary damage state. After a few jumps a mobile interstitial configuration (single and di-interstitial) usually had either encountered a vacancy configuration giving rise to interstitial-vacancy recombination, or another interstitial configuration, giving rise to interstitial clusters. Figure 20 shows the "cleaning up" process for an annealing time of only 37 τ, i.e., the time for an average of 37 jumps per extant mobile interstitial configuration.

Tables XIV and XV give results for an annealing time of 37τ. In Table XIV the initial defect distribution contains no large vacancy cluster but that in Table XV does contain a large vacancy cluster. There was a distinct tendency for large vacancy clusters to be immune to destruction by interstitial-vacancy recombination and for the formation of homogeneously nucleated interstitial clusters. The greater number of recombination events in the spike without a large vacancy cluster and the relative immunity of the large cluster to attrition by interstitial migration, shown in Table XV, are typical features of the annealing process as given by a computer simulation. These results suggest that, in pure iron, the room-temperature neutron-irradiation damage state would be predominantly made up of large vacancy clusters and interstitial clusters. Quali-

TABLE XIV. Defect annealing in a 2.5-keV α-iron displacement spike via interstitial motion. No large vacancy cluster in the initial defect distribution. τ is the mean interstitial jump time.

Start, $t=0$	$t=37\tau$
30 i_1 10 v_1	8 i_1 5 v_1
i_2 2 v_2	2 i_2 v_2
v_3	i_4 v_4[a]
v_4	v_5
v_5	16 recombination events
v_6	

[a] From $v_6+2i_1 \rightarrow v_4$.

TABLE XV. Defect annealing in a 2.5-keV α-iron displacement spike via interstitial motion. A large vacancy cluster is present in the initial defect distribution. τ is the mean interstitial jump time.

Start, $t=0$	$t=37\tau$
28 i_1 7 v_1	7 i_1 4 v_1
v_2	i_2 v_4
v_5	2 i_3 v_{13}
v_{14}	i_6
	7 recombination events

tatively, this particular type of damage state is the same as that observed in neutron-irradiated platinum and tungsten by Attardo and Galligan[42] using the field-ion microscope.

Three causative factors were noted which contributed to the relative immunity of large vacancy clusters to attrition during interstitial migration: (1) One would expect that the outer members of a large vacancy cluster shield the inner members from recombination with migrating interstitials. This effect was observed. (2) As mentioned previously, a significant fraction of the interstitial population in a displacement spike appears at the surface of the spike; the core of the spike tends to be vacancy-rich. The region between the interstitial-rich surface and the large vacancy clusters in the core is populated by small vacancy-cluster configurations and is vacancy-rich. These intervening, small configurations serve to shield the core from the interstitial source at the surface of the spike. In addition, some of the surface interstitials migrate outward into the undamaged crystal region surrounding the spike. (3) A requisite condition for the formation of a large vacancy cluster is that the atoms displaced as it forms be transported a greater average distance from their initial positions than is the case for smaller configurations. This is accomplished directly, for example, by channeling or quasichanneling, the latter being the dominant direct mode. This can also be accomplished, in effect, purely as a statistical consequence of there being a Frenkel-pair instability region. This indirect process has been studied by Lück and Sizmann[28] for electron irradiation of copper on the basis of a model in which vacancies and interstitial atoms are randomly created in a crystal and vacancy-interstitial recombination is determined by a Frenkel pair instability region. The resulting segregation of defect types and cluster formation given by this model is clearly illustrated in a motion picture made by these authors.

By cutting off the range of the attractive interaction between interstitials beyond the second-neighbor distance, we have undoubtedly underestimated the degree of interstitial clustering. In this regard, interstitial-interstitial attraction at separation distances beyond the second neighbor distance can occur when the Erginsoy-Vineyard potential is used. However, these interactions are generally weaker than the first- and second-neighbor distance interactions. The neglect of these longer range interstitial-interstitial interactions does not weaken the conclusions we have drawn regarding either the predominantly defect-cluster damage state produced in a pure material at a finite temperature or the relative immunity of large vacancy clusters to attrition during interstitial migration. A more detailed account of the results obtained by simulating defect annealing on a computer will be given at a later time. The brief description given here was included to illustrate how computer simulations of displacement spike production at 0°K can be used to estimate the damage state produced at a finite temperature.

[42] M. J. Attardo and J. M. Galligan, Phys. Rev. Letters **14**, 641 (1965); Brookhaven National Laboratory Report No. BNL 9909, 1966 (unpublished); M. J. Attardo (private communication).

8. SUMMARY AND CONCLUSIONS

1. The displacement efficiency of a primary knock-on atom (PKA) in tungsten, α-iron, and copper was a monotonically decreasing function of the PKA initial energy. In α-iron and tungsten, this was caused by damage production interference among different parts of a cascade and by long-range channeling. Interference effects accounted for 97% of the decrease in α-iron. All of the decrease of the displacement efficiency in copper was caused by interference effects.

2. At and above 2.5 keV, the quasichanneling probability per knock-on atom in α-iron was sufficiently large (0.05–0.24) that the collided-atom volume exhibited preferred orientation along ⟨100⟩ and ⟨110⟩ directions, the latter being the most prevalent. Long-range self-channeling also exhibited a preference for ⟨110⟩ directions, apparently due to the insensitivity of the range in this channel to the starting position. The range in ⟨100⟩ channels dropped off precipitously when the starting point was moved away from the central position on the channel axis.

3. The volume of the correlated motion recombination region in α-iron should be at least 62Ω at 120°K. This is slightly more than twice the size (30Ω) of the recombination region at 0°K. The α-iron recombination region could conceivably grow to 90Ω at temperatures above 120°K.

4. The displacement density in an isolated displacement spike produced in α-iron at 0°K appears to be saturated.

5. Annealing simulations indicated that if a PKA would produce a spike containing large vacancy clusters (10 or more vacancies) at 0°K in α-iron, then it would produce damage which would survive thermal annealing during irradiation at temperatures up to 250°C.

6. The diameter of the simulated collision cascades in α-iron, tungsten, and copper was determined by the ranges of quasichanneled higher order knock-on atoms rather than by the range of the initiating PKA.

7. The damage state produced in pure metals should be a collection of interstitial clusters and vacancy clusters and the distribution of interstitials in a primary state favors rapid homogeneous nucleation of interstitial clusters at finite temperatures.

ACKNOWLEDGMENTS

D. G. Besco and N. R. Baumgardt wrote the computer programs used to perform the displacement-spike production and annealing calculations. The translation of computer printout into cascade trajectory, collided atom, and damage maps was done by C. M. Schnur and

J. A. Mehne. The author is greatly indebted to C. Erginsoy and G. H. Vineyard for their provision of GRAPE program decks and to R. A. Johnson for his provision of "Johnson's Program" decks. Technical discussions with J. W. Corbett, C. Erginsoy, R. A. Johnson, B. Ralph, W. F. Schilling, G. H. Vineyard, and T. O. Ziebold were particularly rewarding.

APPENDIX

An interatomic potential for tungsten was constructed which had the same form as does Potential III of Erginsoy *et al.*[7] for α-iron. It consisted of an exponentially screened Coulomb potential for $r \leq 1$ Å joined to a simple exponential for $r > 1$ Å

$$\phi(r) = (24500/r)\exp(-4.55r), \quad r \leq 1 \text{ Å};$$
$$\phi(r) = 24500\exp(-4.55r), \quad r > 1 \text{ Å}.$$

This potential is compared with the Bohr, Girifalco-Weizer,[43] Johnson,[10] and Thomas-Fermi potentials in Fig. 21. At small separations distances ($r < 0.4$ Å)$\phi(r)$ fits the Thomas-Fermi potential for tungsten. It is equal to the Morse potential of Girifalco and Weizer at $r = 1$ Å and to Johnson's potential at 2.2 Å.

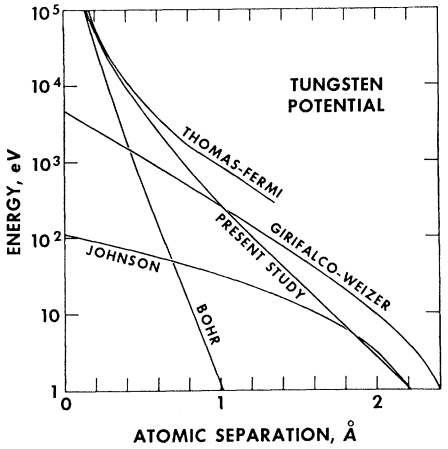

FIG. 21. Tungsten potential used in the present study compared with two high-energy and two low-energy potentials for tungsten.

[43] L. A. Girifalco and V. G. Weizer, Phys. Rev. **114**, 687 (1959).

PHYSICAL REVIEW VOLUME 150, NUMBER 2 14 OCTOBER 1966

Crystal Dynamics of Potassium. I. Pseudopotential Analysis of Phonon Dispersion Curves at 9°K

R. A. COWLEY, A. D. B. WOODS, AND G. DOLLING
Chalk River Nuclear Laboratories, Chalk River, Ontario, Canada
(Received 23 May 1966)

The frequencies of normal modes of vibration of potassium at 9°K have been measured by inelastic-neutron-scattering techniques. Certain selected frequencies are (units 10^{12} cps): H_{15} 2.21±0.02, P_4 1.78$_5$ ±0.02, N_1' 2.40±0.04, N_3' 1.50±0.02$_5$, and N_4' 0.53±0.02. The results are very similar, apart from a scale factor 1.65, to those for sodium. Analysis of the results has been carried out in terms both of conventional Born–von Kármán models and of potential functions defined in reciprocal space. A fifth-neighbor, axially symmetric force model has been used to compute the frequency distribution function for the normal modes and the associated heat capacity. The reciprocal-space analysis was performed in two ways: (a) in terms of a total potential function, whose Fourier transform is the effective interatomic potential between "neutral pseudo-atoms" of potassium, and (b) in terms of the screened pseudopotential for the conduction-electron–ion interaction. Analysis (a) shows that a wide variety of interatomic potentials, both with and without long-range oscillatory character, can be found which give a satisfactory fit to the results. These potentials are compared with those obtained from an analysis of x-ray scattering data for liquid potassium. The pseudopotentials obtained from analysis (b) are in good agreement with that derived by Bortolani from the Heine-Abarenkov model. A reanalysis of the phonon dispersion curves for sodium leads to very similar conclusions, confirming earlier work by Cochran.

1. INTRODUCTION

THE crystal dynamics of metals has received considerable experimental and theoretical attention over the past decade. A large amount of experimental information on dispersion relations $\nu(\mathbf{q})$ of frequency ν versus wave vector $\mathbf{q}$ exists for a number of metals, while theoretical attention has been concentrated principally on the alkali metals.[1] Measurements of $\nu(\mathbf{q})$ for sodium[2] showed that while quite long-range effective forces were present, they were not very strong, and no

[1] For a general review of phonon dispersion curves in metals see G. Dolling and A. D. B. Woods, in *Thermal Neutron Scattering*, edited by P. A. Egelstaff (Academic Press Inc., New York, 1965), Chap. V.

[2] A. D. B. Woods, B. N. Brockhouse, R. H. March, A. T. Stewart, and R. Bowers, Phys. Rev. **128**, 1112 (1962).